ICES Journal of Marine Science, 59: 000–000. 2002
doi:10.1006/jmsc.2002.1282, available online at http://www.idealibrary.com on IDEAL®

Remote sensing of capelin and other biological features in the North Pacific using lidar and video technology

Evelyn D. Brown, James H. Churnside, Richard L. Collins, Tim Veenstra, James J. Wilson, and Kevin Abnett

Brown, E. D., Churnside, J. H., Collins, R. L., Veenstra, T., Wilson, J. J., and Abnett, K. 2002. Remote sensing of capelin and other biological features in the North Pacific using lidar and video technology. – ICES Journal of Marine Science, 59: 000–000.

We evaluated airborne remote sensing, using lidar and colour digital video, in the North Pacific in 2000. Specific objectives were (1) to determine lidar depth-penetration range, (2) to develop ocean colour indices as a proxy for depth penetration and Chl *a*, (3) to compare lidar with acoustic and net-sampling data, (4) to define diurnal variability over large areas, and (5) to evaluate strengths and weaknesses. Depth penetration ranged from 18 to 50 m in non-silty water, with lowest values observed inshore by day and highest values on the continental shelf at night. A green index, derived from the three-band video data, was significantly related to depth penetration and was in general agreement with SeaWiFS satellite Chl *a* values. Significant correlations with acoustics data were obtained in an area with a high concentration of capelin, *Mallotus villosus* (Müller). The day and night distributions of two capelin locations are shown. At a number of zooplankton sampling stations, there was general agreement between densities derived from lidar and vertical net tows. We discuss the spatial patchiness of capelin and zooplankton, ramifications of those distributions on survey design and sampling, strengths, weaknesses, and future research direction for aerial remote sensing.

Keywords: aerial survey, capelin, lidar, *Mallotus villosus*, ocean colour, remote sensing.

Received 12 September 2001; accepted 9 May 2002.

E. D. Brown: University of Alaska Fairbanks, PO Box 757220, Fairbanks, Alaska 99775-7220, USA; tel: +1 907 4745801; fax: +1 907 4741943; e-mail: ebrown @ims.uaf.edu. J. H. Churnside and J. J. Wilson, NOAA Environmental Technology Laboratory, R/E/ET1, 325 Broadway, Boulder, Colorado 80303, USA; tel: +1 303 4861840; fax: +1 303 4973577; e-mail: James.H.Churnside@noaa.gov and J.J.Wilson@noaa.gov. R. L. Collins and K. Abnett: University of Alaska, Fairbanks, Geophysical Institute, PO Box 757320, Fairbanks, Alaska 99775-7320, USA; tel: +1 907 4747607; fax: +1 907 4747290; e-mail: richard.collins@gi.alaska.edu; kevin@giseis.alaska.edu. T. Veenstra: Airborne Technologies Inc., PO Box 879050, Wasilla, Alaska 99687, USA; tel: +1 907 3571500; fax: +1 907 3571501; e-mail: tveenstra@gci.net. Correspondence to E. D. Brown.

Introduction

Ecosystem approaches to fisheries research on schooling pelagic fish such as capelin, *Mallotus villosus* (Müller), require new, cost-effective methods for broad-scale assessment of distribution, abundance, and ecological associations. The patchy and contiguous distribution of such fish requires large numbers of sampling units or transects to achieve statistical validity of assessments if *a priori* information is not available (Cram and Hampton, 1976; Fiedler, 1978; Barange and Hampton, 1997). Ship survey methods are slow and therefore costly, have limited access to nearshore areas where fish often aggregate, and generally sample narrow swaths of water. When fish schools are near the surface, acoustic biomass estimates can be unrealistically low (Vilhjálmsson, 1994). Ship and net avoidance can confound biological assessments of fish and ecological research on the relationships between predators and their fish prey (Aglen and Misund, 1990; Olsen, 1990; Logerwell and Hargreaves, 1996).

Airborne visual surveys coupled with remote sensing instrumentation can eliminate limitations of traditional ship survey methods and have added advantages. Owing to high-speed data collection, the cost per km from aircraft is 10% (or less) that of a ship survey. In a single survey (<8 h), aircraft can cover a study area that would require a week or more for a vessel. Aircraft allow access to both shallow and deepwater regions, and biological features are observed *in situ* without disturbance of biological structure. Because of the near-synoptic view provided by aerial surveys, the integration of airborne data to satellite imagery is more appropriate than is the integration of ship data to satellite imagery. Sea surface temperature and ocean colour data obtained from aircraft-mounted infra-red radiometers (Shaw *et al.*, 2001) and colour imagers or videos are equivalent to the same measurements from Advanced Very High Resolution Radiometers (AVHRR) and Sea-Viewing Wide Field-of-view Sensor (SeaWiFS) satellite imagery (Maffione, 2001). The large number of cloudy days over the North Pacific is a limitation for using AVHRR and SeaWiFS, so data from airborne remote sensing may be particularly useful for interpolating missing or low-resolution data from satellites. Therefore, aerial data can expand the ability to assess pelagic fish such as capelin ecologically, by allowing measurements of processes with varying spatial and temporal scales and by integrating distribution information with other remotely sensed data. The accuracy of remotely sensed data is appropriately validated, interpreted, and scaled by data collected meanwhile on the surface. Some errors can be defined through proper statistical treatment of the results.

Lasers and multi-spectral imagers are not new to ocean science (Hunter and Churnside, 1995). Blue-green light propagates to depths up to 100 m (Squire and Krumboltz, 1981) and green lasers have been applied in the form of lidar (light detection and ranging), where photon backscatter is collected from light reflecting off biological targets in the water column. Although numerical algorithms for lidar detection of fish were established more than 20 years ago (Murphree *et al.*, 1974), modelling of signal-to-noise ratio, estimation of fish abundance, and statistical treatment of lidar data is a continuing area of research (Krekova *et al.*, 1994; Mitra and Churnside, 1999; Lo *et al.*, 2000). Target strength is a function of green-light reflectivity and has been measured on frozen samples of several fish species (Churnside and McGillivary, 1991), and live sardines in a tank experiment (Churnside *et al.*, 1997). Airborne lidar has also been used to detect subsurface oceanic scattering layers (Hoge *et al.*, 1988). In the early 1990s, the Fish Lidar Oceanic Experimental (FLOE) system was constructed from off-the-shelf components, and improvements were made to signal-processing techniques used to discriminate fish returns from small particles in the water (Churnside *et al.*, 1998, 2001a). The FLOE system penetrates depths up to 50 m, and has been used off the coast of California to survey anchovy and sardine (Hunter and Churnside, 1995; Churnside *et al.*, 1997; Lo *et al.*, 2000), and has more recently been used to measure plankton, squid, and marine mammals (Churnside *et al.*, 2001a). Comparisons of lidar with acoustic data have been very encouraging, and these methods can produce similar results (Churnside *et al.*, 2001b; Figure 1).

In 2000, the FLOE system was coupled with a colour digital video in a single platform and both were evaluated as marine ecological research tools in the North Pacific. The specific objectives of the pilot study were to (1) determine depth penetration in Subarctic waters, (2) develop an ocean colour algorithm from a linear combination of spectral bandwidths as a proxy of both depth penetration and Chl *a*, (3) compare densities of fish schools and zooplankton aggregations obtained from lidar with those obtained from shipboard acoustics and nets, (4) compare day vs. night data collected within a period of 24 h over the same survey path, and (5) evaluate the potential uses and limitations of the instrument package for marine research applications. The choice to test the capabilities of the colour digital video over a multispectral imager concerned cost and compactness. Multispectral imagers are expensive and bulky and therefore difficult to combine with other instrumentation in a single platform. If meaningful results could be produced from the three wide bands (red, green, blue) or narrower bands obtained through spectral filters on the colour video, the economy and convenience of obtaining image data from aircraft could be substantially improved.

Methods

In 2000, the FLOE system (Churnside *et al.*, 2001a) and a colour digital video camera were mounted downlooking from the port side of a twin-engine aircraft (Figure 2, right) and field-tested at three separate locations in the eastern North Pacific. The FLOE system was mounted over a hole in the belly of the aircraft and the camera was mounted through a hole cut in an adjacent bubble window (Figure 2, left). Both instruments were aimed 15° off vertical to minimize specular reflections from the sea surface and to permit visual observations overlapping the lidar and image data. The altitude and airspeed were standardized at 305 m and 222 km h^{-1} (120 knots) respectively for all locations, to eliminate the variability introduced by variable data-collection height and rate. Data from each instrument were stored electronically and geo-referenced at 1 s intervals by Global Positioning System (GPS). Roll, pitch, and yaw of the aircraft were also measured to correct for changes in capture angle during post-processing. In each location, aerial surveys

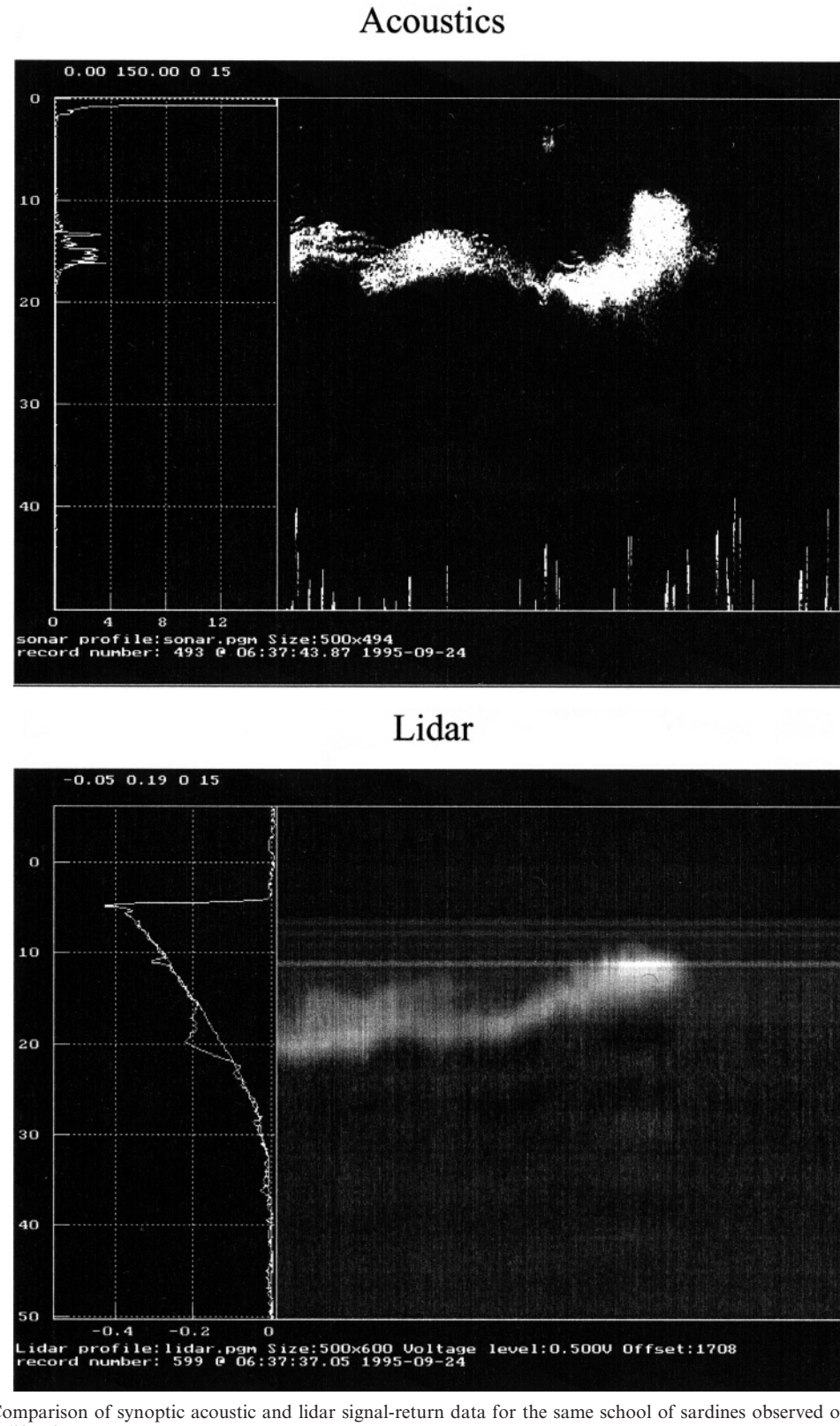

Figure 1. Comparison of synoptic acoustic and lidar signal-return data for the same school of sardines observed off the coast of southern California.

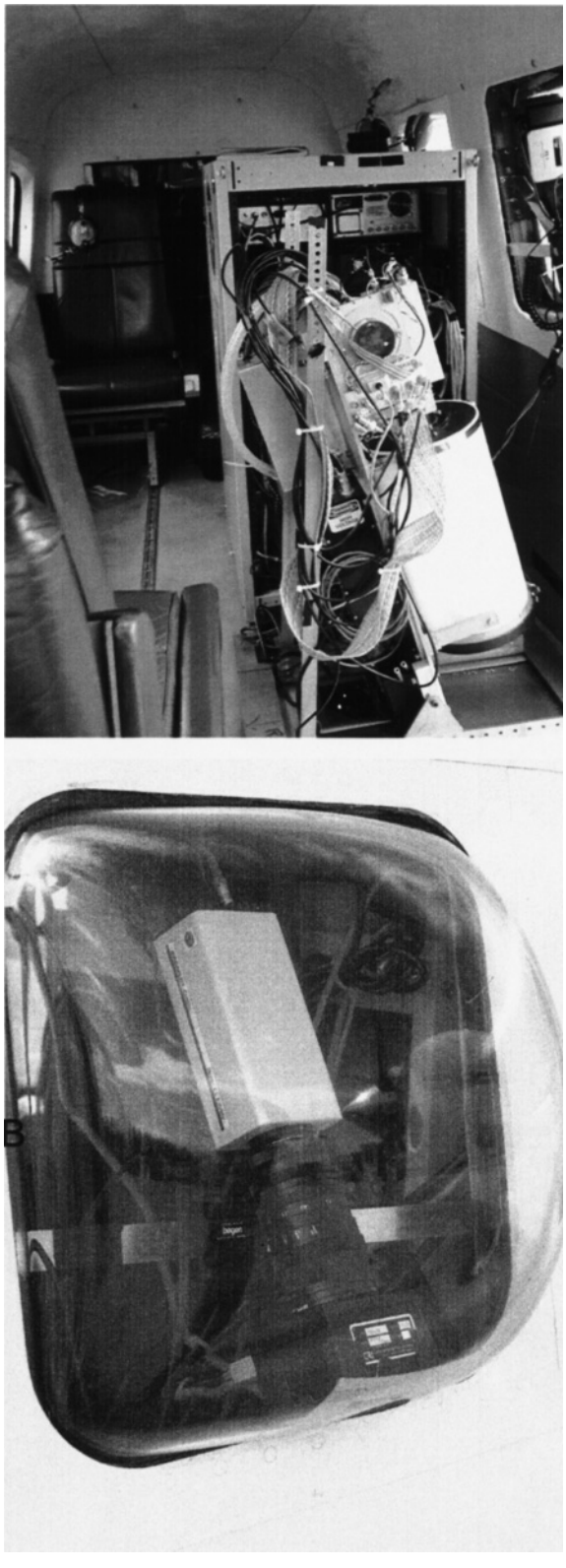

were coordinated with shipboard research programmes that could provide identifications of biological targets for interpretation of aerial data. In addition, these programmes provided acoustic backscatter measurements, zooplankton densities, Chl *a* concentrations, light attenuation, and other physical measurements for comparison with aerial data.

The components and settings of FLOE are described in detail by Churnside *et al.* (2001a), but are summarized here for easy reference. The FLOE system is a non-scanning, radiometric lidar with three major components: (1) the laser and beam-control optics, (2) he receiver optics and detector, and (3) the data collection and display computer. The laser is linearly polarized and the beam diverged, using a lens in front of the laser, to meet eye-safety standards established for marine mammals (Zorn *et al.*, 2000). During the day, a narrower divergence filter is used than at night, when it is three times wider. The narrow filter minimizes the amount of background light entering the receiver, but effectively limits the penetration depth of laser light (Gordon, 1982). A polarizer in front of the telescope selects the cross-polarized component of the reflected light, thus maximizing contrast between fish and smaller light-scattering particles (Churnside *et al.*, 1997; Lewis *et al.*, 1999). The telescope collects the light onto an interference filter to reject background light. As with the divergence filter, a narrow interference filter is used by day and a wider one at night. An aperture at the focus of the primary lens also limits background light by limiting the field of view of the telescope to match the divergence of the transmitted laser beam. The resulting light is incident on a photomultiplier tube, which converts the light into an electrical current. For the night-time receiver, the active area of the photomultiplier tube is the field-stop aperture. By day, a separate aperture is used, and the light is transferred to the photomultiplier tube by a second lens. The combination of divergence lens size, field-of-view setting, interference filter width, and altitude flown in 2000 determined the spot diameter or sampling swath at 5 m by day and 15 m by night. The photomultiplier tube output is passed through a logarithmic amplifier to increase the dynamic range of the signal. A 50-Ω load resistor converts the current in a voltage, which can be digitized in the computer.

The high-resolution, colour digital video camera had an adjustable focal length as well as frame-capture rate, and was equipped with a telescoping lens as well as

Figure 2. (Top) Mounting configuration of the FLOE system and video camera. The telescope, with its angled orientation, is in the foreground; the mounting rack housing the remainder of the electronics is immediately behind the telescope. The bubble window housing the colour video camera can be seen in part to the right of the telescope. (Bottom) Close-up of the video camera with the multispectral filter attached.

tunable, multispectral filters capable of capturing 10 different bandwidths within the visual range. Without the filter, the available bandwidths were the broad red, green, and blue outputs from the three-colour chip within the camera. The image swath width depended upon the altitude and focal length, and ranged from 150 to 200 m at 305 m altitude. The image pixel resolution was approximately 6 cm at the airspeed and altitude flown in 2000. With custom software, the image data were binned to specified sizes and geo-referenced at the centre of each bin; normalized colour pixel values were then assigned to each bin.

Lidar files were large, representing an array with 1000 depth bins of 0.1 m extent and 2000 shot returns. The laser pulsed light 30 times per second, so a file contains 66 s of data representing about 4.5–5 km of explored distance (airspeed-dependent). A typical flight can acquire several hours of data, yielding some 150–200 data files. Files were first corrected by the surface echo, then the median return per bin and slope of background backscatter was estimated so as to calculate signal over noise. The backscatter signals were normalized to the background backscatter or median backscatter, for comparison with other bins. Figure 3 illustrates the processing steps involved for interpreting the received signal from a laser shot. The background signal, the total received averaged signal (root-mean-square averaged), and the median signal were often plotted geographically to aid in batch-processing, using geo-referenced notes or auxiliary data collected during a survey.

Penetration depth was determined by a threshold depth, below which meaningful signal could not be discriminated from noise. Because light attenuates in the water column, a return signal is weaker with increasing depth, so a threshold above the signal produced by noise alone is selected. Using the plotted median of the lidar return over several hundred shots of the data, threshold noise could be easily identified, and the depth at which this curve crosses the threshold is the penetration depth. This is illustrated in Figure 3b, where the return signal becomes noisy, corresponding to a penetration depth of about 30 m. That depth was at a signal current of 1×10^{-9} A, which is the threshold signal used to filter the data from shots associated with the estimated median.

Lidar penetration is known to be less in water that is greener because of its higher concentration of phytoplankton. We wanted to define this functional relationship. In addition, we wanted to test the feasibility of developing an ocean colour index from the colour video data as a proxy measurement of Chl *a*. To accomplish the first task, a green index was estimated from the colour video data and plotted against penetration depth. The level of significance and correlation coefficient was determined. For the second task, the green index was compared with SeaWiFS imagery rather than Chl *a* data, which were unavailable at the time of writing. The green index (G) was estimated as the green-only component of a pixel or range of pixels, normalized by the total intensity from that pixel or pixel range. The total intensity is estimated as the sum of the red, green, and blue components. Thus, a grey image would produce a green index of 0.33, independent of its intensity.

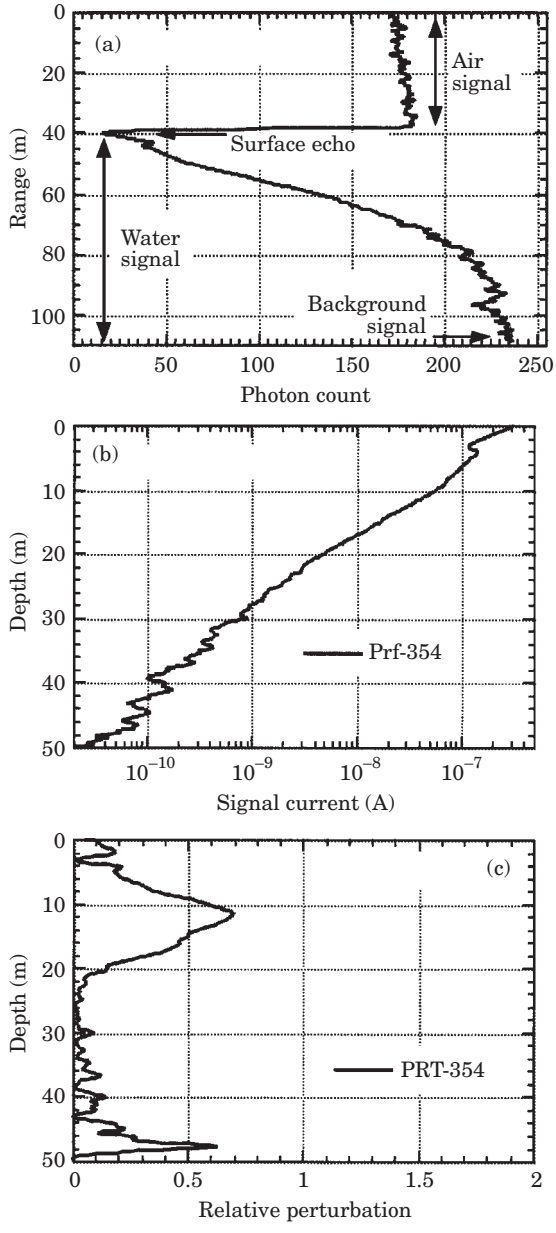

Figure 3. Characteristics of the signal received from a single transmitted laser pulse collected at an altitude of 250 m over Prince William Sound, Alaska: (a) photon counts from the raw signal detector vs. echo by distance from the plane; (b) the signal below the surface echo in terms of the linear detector current vs. depth; (c) the total signal over a 1000-shot-median background (b – median) for this single-shot return.

For comparing fish and zooplankton densities, acoustic backscatter was regressed with lidar backscatter. Acoustic data were available from two locations within one of the three regions surveyed. Acoustic and lidar data were not collected at the same along-track resolution, and binning was necessary for quantitative comparisons. In addition, logistical problems prevented perfect temporal overlap and forced different directions of travel along and through the ship transects. As a result, data from the two locations could only be compared at two spatial scales with two different time-lapses. For each of the locations, lidar backscatter was regressed with acoustic backscatter for each of the four transducer frequencies. There were four acoustic transducer frequencies available (43, 120, 200, and 420 kHz), that were multiplexed from a single tow body (K. O. Coyle, University of Alaska, Fairbanks, pers. comm.). For each frequency, acoustic data were converted from decibel to numeric values and then integrated within each bin through the penetration depth range of overlapping lidar data. The integrated numerical value was then divided by the mean target strength of -70 dB (K. O. Coyle, pers. comm.) to get total acoustic backscatter per bin. Lidar backscatter was estimated as the sum of the total signal over background (Figure 3c) within a given bin.

For an additional comparison of zooplankton densities, lidar backscatter was compared with zooplankton density from vertical net tows. At the time of writing, net-sampling results were available for only one of the three regions surveyed (M. Sturdevant, National Marine Fisheries Service, Juneau, Alaska, pers. comm.). There was good spatial and temporal overlap between the aerial surveys and zooplankton sampling, and three aerial passes were made within a 2 h period over each sampling station. GIS software was used to link the locations in time and space. Lidar data were queried within a 2.5 km block around the zooplankton stations. The average integrated lidar signal, within a depth range of 0–20 m, was estimated for each block and aerial pass, then compared with the appropriate zooplankton settled volume (cm^3). Zooplankton was collected during daylight and was therefore compared only with daytime aerial survey data.

For the day vs. night comparison, we chose to illustrate diurnal differences in distribution of capelin and co-occurring biological organisms. These illustrations were from lidar surveys conducted at or near the acoustic and net-capture sites in the Gulf of Alaska, where validation data were available.

Results

During July and August 2000, approximately 15 000 km were covered in a little more than 65 h during 10 non-consecutive survey days in three spatially distinct regions: nearshore waters off southern British Columbia, nearshore waters off northern Southeast Alaska, and from Prince William Sound to the continental shelf break of the adjacent Gulf of Alaska. A variety of biological features and water body types were observed owing to the wide spatial coverage of the combined surveys.

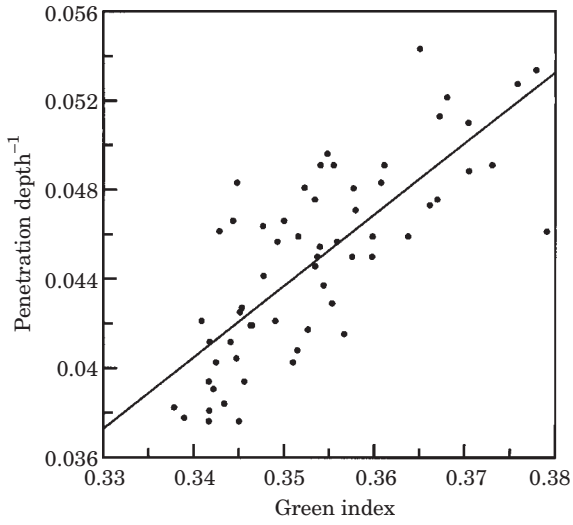

Figure 4. The green index calculated from the colour video data vs. the inverse of the penetration depth for the flight on 20 August 2000. The threshold for this flight was a signal current of 3×10^{-9} A. The line is a linear fit, given by $d^{-1} = 0.320G - 0.0682$, where d is the penetration depth and G is the green index. The correlation coefficient for the relationship is 0.77 ($p = 0.0001$).

Depth penetration ranged from 18 to 50 m in non-silty water, with a major bifurcation of depth penetration between day and night and between nearshore and deeper, shelf waters. Penetration depths at night were often double those by day, but lowest in silty river plumes (<10 m), intermediate in inside passages, bays and fjords (18–30 m), and highest in open ocean, continental shelf waters (25–50 m). The best penetration range was obtained over the mid-shelf off the northern Gulf of Alaska.

The inverse of depth penetration was significantly ($p = 0.0001$) related to the green index (G; Figure 4), confirming the relationship between ocean colour or primary productivity and the attenuation of light in the water column.

The green index for 20–24 August 2000 was plotted with a SeaWiFS composite image for August (Figure 5). It ranged from 0.34 to 0.40 for the northern Gulf of Alaska. Not surprisingly, higher values of G were associated with greener water, indicative of higher productivity in terms of Chl *a*. SeaWiFS and video ocean colour data generally agreed, both indicating greater

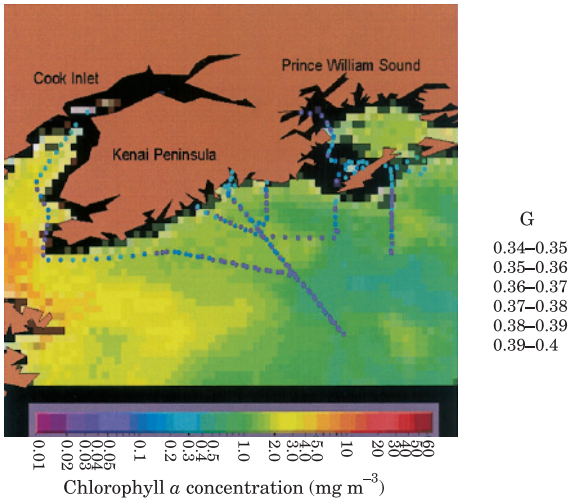

Figure 5. The green index (G), calculated as the green-band output from the colour video normalized by the total intensity (sum of red, green, and blue bands), for 20–24 August 2000, plotted over a SeaWiFS (NASA/Goddard Space Flight Center and ORBIMAGE) composite image for August 2000 in the Gulf of Alaska and adjacent fjords. Higher values of G represent greener, more productive waters.

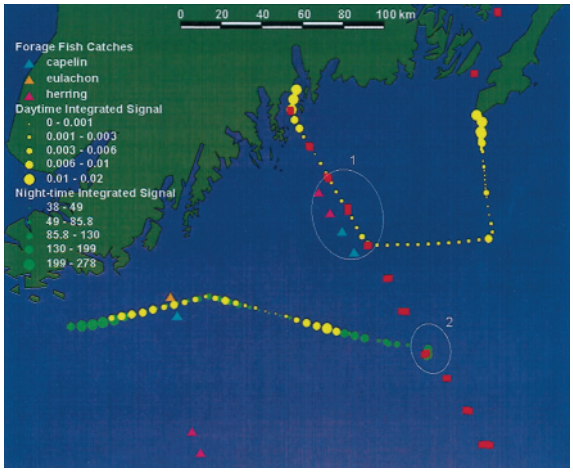

Figure 6. Relative strength of received signal by location for daytime (yellow) and night-time (green) lidar surveys. The overlapping regions of acoustic surveys (red squares) and lidar surveys are identified within the white ovals. Net captures of capelin (blue triangles), eulachon *Thaleichthys pacificus* (orange triangles), and herring (red triangles) are also identified.

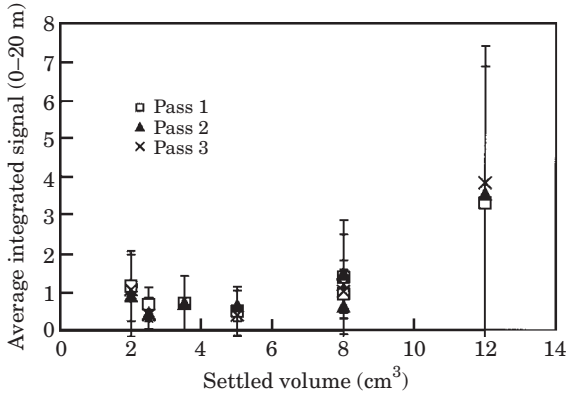

Figure 7. Average lidar signal integrated over the upper 20 m from a 2.5-km-square block plotted against zooplankton settled volume (cm^3) at corresponding stations within each block. The three marks indicate separate lidar measurements made during each of three aerial passes over the stations, and the error bars indicate 2 × s.d. of signal about the means.

phytoplankton production in fjords or nearshore than offshore. Data from the aerial surveys had better coverage nearshore and in fjords because flights took place under clouds. Cloud cover was frequent in the area, and resolution from the SeaWiFS sensor is poor near land owing to a confounding of ocean colour with land colour values.

The comparisons of lidar with acoustic signal produced mixed results. For area 1 (Figure 6), the bin size was 400 m, there was a 7–8 day delay between acoustic and lidar surveys, and lidar data were available by day whereas acoustic surveys were carried out at night. There was no correlation between the integrated signal from any of the four acoustic frequencies and the lidar signal. For area 2 (Figure 6), both surveys were conducted at night, the bin sizes were larger at 4 km, and the time delay was reduced to four days. Data from all four acoustic frequencies were significantly ($p \leq 0.0002$) related to lidar data, with correlation coefficients (r) ranging from 0.550 to 0.592. The best correlation was with the 200 kHz frequency.

There was general agreement between zooplankton settled volume and the average integrated lidar signal over the seven sampling stations examined. Average signal was low at stations with low settled volumes, and the station with the biggest settled volume also had the highest average signal (Figure 7). Although there was not much variation in average lidar signal between the three aerial passes, there was considerable variability in signal within a given block around a station. Within-block variability of signal appeared to increase with zooplankton density. This increasing variability with density (Figure 8) appeared to result from a high degree of spatial patchiness and the variation in density within patches.

There was considerable difference between day and night in the observed distribution of capelin schools, zooplankton layers, and other unidentified targets. The high capture rate allowed a true diurnal comparison of a large region, such as the 300 km wide continental shelf in the study area, in a single 24 h period. In 2000, capelin were anecdotally reported to be particularly abundant in the Gulf of Alaska. Over the shelf, capelin were mainly at locations where the bottom depth ranged from 100 to

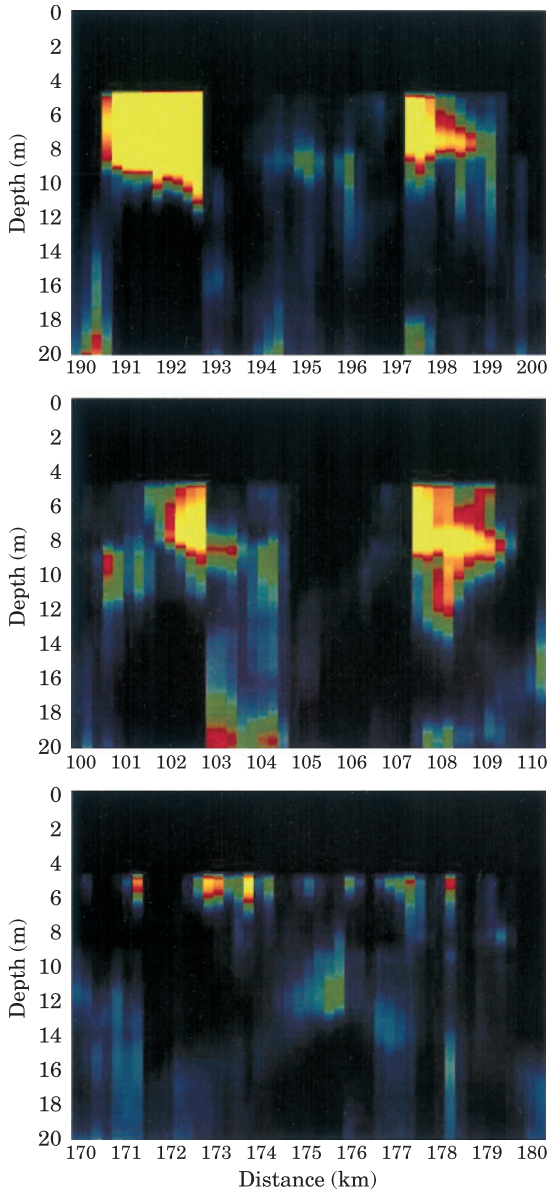

Figure 8. Plotted arrays of daytime lidar data representing interpreted relative signal strength vs. depth along a 10 km segment of the aerial transect associated with high zooplankton density, according to net-sampling results (top), medium density (middle), and low density (bottom). Strongest relative signal is yellow, weakest is green, and background signal is black.

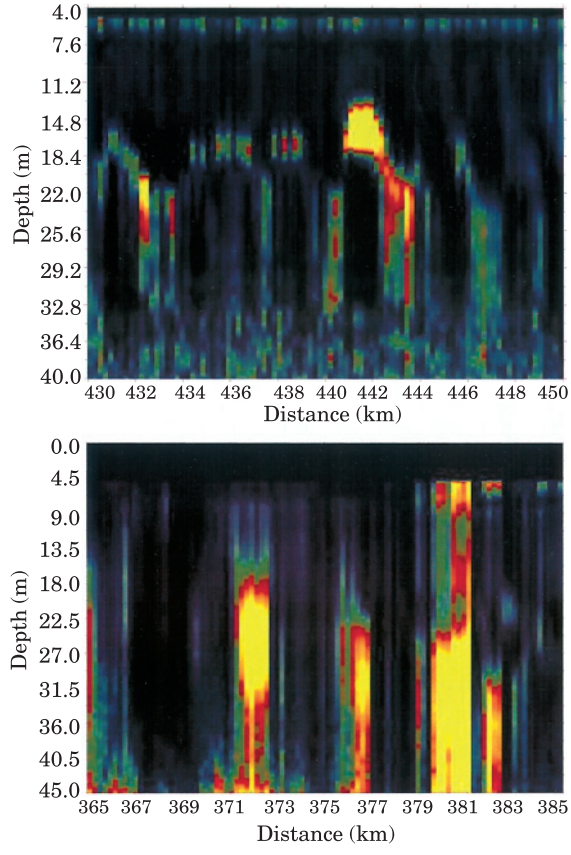

Figure 9. Plotted arrays of lidar data representing interpreted relative signal strength vs. depth along a 20 km segment of the aerial transect overlapping with the acoustic survey in area 2 (Figure 6) during the day (top) and along the same 20 km at night (bottom).

180 m (K. O. Coyle, pers. comm.). Therefore, the capelin observed in the upper 50 m probably represented only part of the total population present. Nevertheless, many large schools were detected with lidar, especially along the flight tracks shown in Figure 6. For area 2 (Figure 6), schools of capelin were observed in the upper 50 m by day, but in larger schools and in much higher densities over the same region by night (Figure 9). West of the acoustic stations but near a net-sampling site, capelin schools appeared to be smaller and were mixed with other unidentified targets (Figure 10). In addition, there was a higher concentration of targets in the upper 50 m by day than by night. However, capelin schools generally appeared to extend >1 km in along-track distance, were often 20 m thick or thicker, and aggregations of schools appeared to extend to about 10 km.

Discussion

The strength of airborne remote sensing for applications in fisheries research and marine ecology appears to be its ability to collect a diverse array of physical and biological data over large regions quickly. A wide array of instruments allows synoptic collection of parameters such as sea surface temperature and salinity, ocean colour, seabird and marine mammal distributions, and the spatial patchiness and density of zooplankton and fish aggregations. The result may lead to better

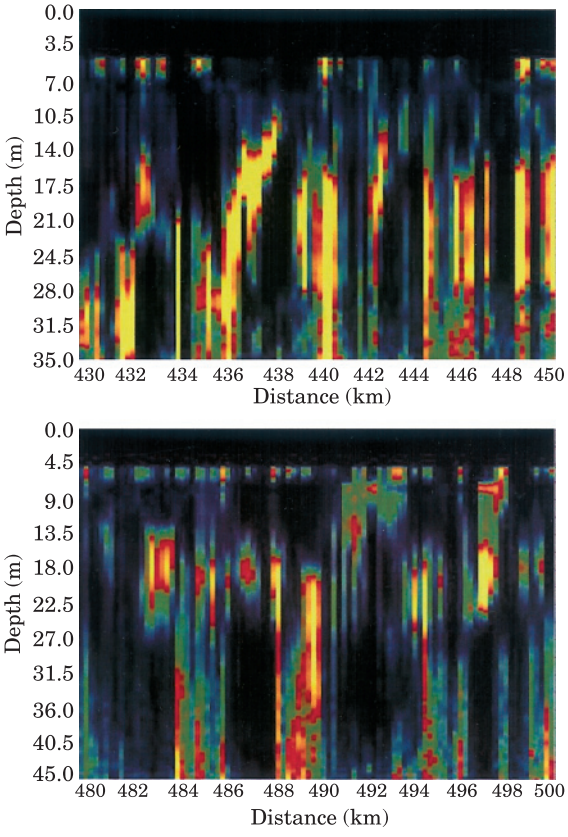

Figure 10. Plotted arrays of lidar data representing interpreted relative signal strength vs. depth along a 20 km segment of the aerial transect associated with capelin and herring catches during the day (top) and along the same 20 km segment at night (bottom).

understanding of biological spatial patchiness and temporal variability.

One weakness of airborne surveys is that most measurements are associated with the near-surface, and in the case of eye-safe lidar, the upper 50 m. In a study using airborne remote sensing, the use of ground-validated information is crucial not only for interpretation of electronic data, but also for subsurface extrapolation. For pelagic fish such as capelin, acoustic measurements from ships would be essential for interpreting the distribution below lidar penetration depth.

Another weakness of airborne remote sensing is the effect of wind and waves on the reliability and variability of the data. Any increase in pitch, roll, and yaw of the aircraft, as well as any increased roughness of the ocean surface as a result of wind can result in reduced ocean penetration, reduced signal-to-noise ratios (Churnside *et al.*, 1997), and a masking of surface features such as seabird flocks or whales.

In evaluating the colour video, the multispectral filter proved of limited use at the altitude flown for lidar surveys. Much of the time, insufficient light entered the camera at the narrow bandwidth allowed by the filter to render an interpretable image. We did not test the multispectral filter at higher altitudes, but there are indications (G. A. Borstad, Borstad Assoc., Sydney, British Columbia, pers. comm.) that it may have performed better.

Once the filter was removed, the utility of processing the green band of the video over total intensity of all three colour bands was demonstrated. The relationship of the green index (G; Figure 4) to the depth penetration of the lidar signal, as well as its apparent relationship with ocean productivity (Figure 5), have implications for lidar data processing, for the delineation of ocean regions by production, and for interpolation of incomplete or missing satellite data. For lidar processing, regions of similar ocean colour probably indicate areas with similar attenuation curves, within which error in estimation of background signal can be minimized. Identifying lidar files for batch processing by regions of similar ocean colour could improve the quality and processing efficiency of lidar data.

The lack of, or moderate correlation between, acoustic and lidar signal could have resulted from the time lag between the two surveys and variability in the distribution of mobile targets, such as capelin, above and below the depth-penetration range of lidar. However, given the correlation in at least one of the regions surveyed (area 2, Figure 6), an assessment or research programme utilizing both acoustics and lidar could be of value. Survey design and precision of abundance estimates for highly contiguous and mobile pelagic fish has been a perennial problem for marine researchers (Fiedler, 1978; Petitgas, 1993; Simmonds and Fryer, 1996; Barange and Hampton, 1997). A coordinated aerial and ship survey could help alleviate such problems. When capelin aggregate near the surface, airborne surveys could cover large regions mapping spatial patchiness, while ships with acoustic capabilities and nets could be directed to sample patches adaptively, providing density estimates, age and size distributions, sub-penetration distribution, and other information needed for extrapolation of airborne data (Lo *et al.*, 2000). Methods to estimate the error of adaptive survey designs are well established (Thompson, 1992). Cost benefits could include a reduction in the overall time needed to survey a region by allocating expensive ship's time to measurements at targeted areas, rather than transecting large areas in search patterns. Added benefits could be a reduction in bias and an increase in precision of abundance estimates. Bias can occur when the movement of schools exceeds the speed of the ship, confounding abundance estimates (Petitgas, 1993). Precision is improved when spatial patchiness is measured and applied in the calculation of distribution and abundance (Petitgas, 1993; Simmonds and Fryer, 1996).

A lack of understanding of spatial patchiness could also impact the precision of estimates of zooplankton density. Spatial patchiness may be especially high nearshore, where local turbulence from tides and eddies can affect zooplankton distribution. In 2000, researchers in Alaska were studying processes affecting growth and survival of juvenile salmon during their early marine phase (J. Orsi, NMFS, Auke Bay Lab, Juneau, Alaska, pers. comm.). Measurements of zooplankton density were crucial in these studies. However, given the high degree of spatial patchiness along with the variability in patch size and density observed at the zooplankton sampling stations in this study (Figure 8), it has to be concluded that density estimates from single net tows may possess a high degree of error that is not being measured. Airborne measurements could be used to map zooplankton patches and to obtain a better understanding of the relationship between growth and movement of fish in these highly variable nearshore regions.

We are expanding the capabilities of airborne remote sensing by adding instruments to the array on the aircraft. Infra-red and microwave radiometers provide synoptic measurements of sea surface temperature and salinity. A light sensor allows better calibration of the effects of cloud cover on the estimation of sea surface temperature and lidar background signal. Infra-red video allows day and night mapping of seabirds and marine mammals coincident with the physical and biological features captured by other instruments. A gated video, synchronized with lidar pulses, captures shadow images of features illuminated by the laser at 1-m depth bins. These images may aid in target identification and so improve signal interpretation. Finally, the addition of a spectral fluorometer (Maffione, 2001) may expand our capability to study ocean optics and plankton community structure.

Our research efforts continue to be focused on ecological assessment and technique development, exploring the incorporation of ocean colour information in lidar processing procedures. We are standardizing and improving the efficiency of processing lidar data, as well as developing the software to allow visualization and analysis of acoustic, video, and other data coupled to lidar measurements. We hope to conduct *in situ* and *in vitro* target-strength studies on fish and zooplankton. Target-strength measurements for lidar are based on optical, rather than acoustic, signatures. In this area, lidar development lags acoustic technology by at least 10 years, so we want to design and build a new lidar system with improved depth penetration and flexible resolution that would allow mapping of much smaller features than is currently possible. Such features could include individual organisms, e.g. migratory salmon and apex predators near the surface in the extreme nearshore, and in freshwater systems. However, the largest obstacle in development may be general acceptance of airborne remote sensing by resource managers, government agencies, and other researchers. Acceptance may include a willingness to alter long-standing survey designs or single-species thinking along with a desire to allocate resources to remote sensing. However, we do recognize that the transfer of technology is not a trivial task and will require a commitment on the part of agencies and other institutions for time and training.

Acknowledgements

This project was funded by the North Pacific Marine Research program at the University of Alaska, Fairbanks. We thank all cooperating shipboard research programs for the coordination and sharing of data, in particular: Drs David Welch, Richard Beamish, and Doug Hay from the Pacific Biological Research Station in Nanaimo, British Columbia, along with the captain and crew of the RV "Ricker"; Drs Tom Weingartner, Ken Coyle, Lew Haldorson, and especially Seth Danielson, all from the Institute of Marine Science at the University of Alaska, as well as Tom Smith and the captain and crew of the RV "Alpha Helix" from the Seward Marine Center in Seward, Alaska; Joe Orsi, Molly Sturdevant, Jim Murphy, Ed Farley, Steve Ignell, and Jack Helle from the NMFS Auke Bay Laboratory in Juneau, Alaska, and the captain and crew of the RV "Cobb". Finally, we thank our talented pilots, Dick Stephanski and Bill Reimer, for keeping us safe in the air, and Tom Blaesing, Commander Northwest Ltd, for providing the twin-engine aircraft.

References

Aglen, A., and Misund, O. A. 1990. Swimming behaviour of fish schools in the North Sea during acoustic surveying and pelagic sampling trawling. ICES CM 1990/B: 38.

Barange, M., and Hampton, I. 1997. Spatial structure of co-occurring anchovy and sardine populations from acoustic data: implications for survey design. Fisheries Oceanography, 6: 94–108.

Churnside, J. H., and McGillivary, P. A. 1991. Optical properties of several Pacific fishes. Applied Optics, 30: 2925–2927.

Churnside, J. H., Sawada, K., and Okumura, T. 2001b. A comparison of airborne lidar and echo sounder performance in fisheries. Journal of the Marine Acoustical Society of Japan, 28: 49–61.

Churnside, J. H., Tatarskii, V. V., and Wilson, J. J. 1998. Oceanic attenuation coefficients and signal fluctuations measured from a ship in the southern California Bight. Applied Optics, 37: 3105–3112.

Churnside, J. H., Wilson, J. J., and Tatarskii, V. V. 1997. Lidar profiles of fish schools. Applied Optics, 36: 6011–6020.

Churnside, J. H., Wilson, J. J., and Tatarskii, V. V. 2001a. An airborne lidar for fisheries applications. Optical Engineering, 40: 406–414.

Cram, D. L., and Hampton, I. 1976. A proposed aerial/acoustic strategy for pelagic fish stock assessment. Journal du Conseil International pour L'Exploration de la Mer, 37: 91–97.

Fiedler, P. C. 1978. The precision of simulated transect surveys of northern anchovy, *Engraulis mordax*, school groups. Fishery Bulletin U.S., 76: 679–685.

Gordon, H. R. 1982. Interpretation of airborne oceanic lidar: effects of multiple scattering. Applied Optics, 21: 2996–3001.

Hoge, F. E., Berry, R. E., and Swift, R. N. 1988. Active–passive airborne ocean color measurement. 1. Instrumentation. Applied Optics, 25: 39–47.

Hunter, J. R., and Churnside, J. M. 1995. Airborne fishery assessment technology: a NOAA workshop report. NOAA Southwest Fisheries Science Center Administrative Report, La Jolla, California, LJ–95–02. 71 pp.

Krekova, M. M., Krekov, G. M., Samkhvalov, I. V., and Shamanaev, V. S. 1994. Numerical evaluation of the possibilities of remote laser sensing of fish schools. Applied Optics, 33: 5715–5720.

Lewis, G. D., Jordan, D. L., and Roberts, P. J. 1999. Backscattering target detection in a turbid medium by polarization discrimination. Applied Optics, 38: 3937–3944.

Lo, N. C. H., Hunter, J. R., and Churnside, J. H. 2000. Modeling statistical performance of an airborne lidar survey system for anchovy. Fishery Bulletin U.S., 98: 264–282.

Logerwell, E. A., and Hargreaves, N. B. 1996. The distribution of sea birds relative to their fish prey off Vancouver Island: opposing results at large and small spatial scales. Fisheries Oceanography, 5: 163–175.

Maffione, R. A. 2001. Evolution and revolution in measuring ocean optical properties. Oceanography, 14: 9–14.

Mitra, K., and Churnside, J. H. 1999. Transient radiative transfer equation applied to oceanographic lidar. Applied Optics, 38: 889–895.

Murphree, D. L., Taylor, C. D., and McClendon, R. W. 1974. Mathematical modeling for the detection of fish by an airborne laser. Journal of the American Institute of Aeronautics and Astronautics, 12: 1686–1692.

Olsen, K. 1990. Fish behaviour and acoustic sampling. Rapports et Procès-Verbaux des Réunions du Conseil International pour l' Exploration de la Mer, 189: 147–158.

Petitgas, P. 1993. Use of disjunctive kriging to model areas of high pelagic fish density in acoustic fisheries surveys. Aquatic Living Resources, 6: 201–209.

Shaw, J. A., Cimini, D., Westwater, E. R., Han, Y., Zorn, H. M., and Churnside, J. H. 2001. Scanning infrared radiometer for measuring the air-sea temperature difference. Applied Optics, 40: 4807–4815.

Simmonds, E. J., and Fryer, R. J. 1996. Which is better, random or systematic acoustic surveys? A simulation using North Sea herring as an example. ICES Journal of Marine Science, 53: 39–50.

Squire, J. L., and Krumboltz, H. 1981. Profiling pelagic fish schools using airborne optical lasers and other remote sensing techniques. Journal of the Marine Technology Society, 15(4): 27–31.

Thompson, S. K. 1992. Sampling, pp. 176–204. John Wiley & Sons, New York.

Viihjálmsson, H. 1994. The Icelandic capelin stock. Rit Fiskideildar, 13: 281 pp.

Zorn, H. M., Churnside, J. H., and Oliver, C. W. 2000. Laser safety thresholds for cetaceans and pinnipeds. Marine Mammal Science, 16: 186–200.